Quantification and Authentication of Edible Oils by ^{1}H NMR Spectroscopy

Combinatorial Analysis of Integral Fingerprints, Multivariate Identity Mapping, and Detection of Adulteration in Avocado, Olive, and Seed Oils

A Process NMR Associates Technical White Paper

John C. Edwards, Ph.D.
Process NMR Associates, LLC
84 Patrick Lane, Suite 115, Poughkeepsie, NY 12603
www.process-nmr.com

July 2026

Abstract

A set of two hundred ^{1}H NMR spectra, acquired on retail edible oils and fats spanning approximately thirty botanical and animal classes, has been reduced to ten integrated resonance regions (designated A through J) that together encode the acyl-chain composition of the triacylglycerol pool. Because each integral is normalized to the glyceryl methylene signal (H, four protons per triacylglycerol, set to 100), every region is expressed on a strict per-molecule basis, and the resulting proton bookkeeping permits the direct recovery of molar fatty-acid composition, mean double-bond number, and iodine value without recourse to derivatization or chromatography. Derived saturated, oleic, linoleic, and linolenic fractions are shown to agree with established compositional ranges across the sample set, and iodine values from roughly 5 for coconut to 182 for flaxseed are reproduced. A systematic combinatorial screen of one hundred fifty-seven single integrals, pairwise ratios, and chemically motivated composite expressions was then evaluated against two objectives: discrimination among botanical classes and quantification of deliberate adulteration. Principal-component analysis of the autoscaled fingerprint accounts for 84.9% of the total variance in three components, and a leave-one-out linear-discriminant model classifies eight reference classes with 83.8% accuracy, the residual error residing almost entirely within the compositionally similar high-oleic group. The difficult separation of avocado from olive oil, for which oleic content is non-diagnostic, is achieved at 93% by a compact three-ratio model exploiting the methylene-distribution ratio D/C1, the bulk-methylene ratio C2/C1, and the olefinic fine-structure ratio I/J. Gravimetrically defined spiking series demonstrate that canola, soybean, and palm each drive the avocado fingerprint along a distinct and chemically interpretable vector, and univariate calibrations against the linolenic (G1), bis-allylic (G1+G2), and olefinic (J+I) families return coefficients of determination above 0.999 with detection limits between 1.6 and 2.3 volume percent. The same coordinates are shown to expose base-oil substitution in commercial "canola and olive oil" blends. The strengths and boundaries of the approach are assessed candidly, including the overlap of avocado with refined high-oleic seed oils, the additive baseline that limits absolute linolenic quantification at low levels, and the fact that squalene and sterol markers lie outside the integrated window and therefore require orthogonal confirmation.

Table of Contents

Abstract **2**
1. Introduction **4**
1.1 Economically motivated adulteration of edible oils 4
1.2 The molecular basis of the oil fingerprint 4
1.3 ^{1}H NMR as a rapid fingerprint of acyl-chain composition 4
1.4 Scope and objectives 5
2. Quality and Authenticity Parameters Accessible by ^{1}H NMR **5**
2.1 The ten diagnostic regions of the edible-oil ^{1}H NMR spectrum 5
2.2 Per-triacylglycerol normalization and proton bookkeeping 6
2.3 Recovery of molar fatty-acid composition 6
2.4 Iodine value and mean unsaturation 7
2.5 Oil-specific marker chemistry 7
3. Materials and Methods **7**
3.1 Sample set and calibration mixtures 7
3.2 Data extraction, normalization, and quality control 8
3.3 Derived-parameter computation 8
3.4 Combinatorial screening 8
3.5 Multivariate analysis 9
4. Results and Discussion **9**
4.1 Molar fatty-acid profiles and iodine values 9
4.2 Correlation structure of the integrals 10
4.3 The master identity maps 10
4.4 Separation of the high-oleic oils and the avocado–olive problem 11
4.5 Principal-component structure of the fingerprint 11
4.6 Combinatorial ranking of diagnostic combinations 12
4.7 Adulteration drives distinct and interpretable vectors 13
4.8 Quantitative calibration and detection limits 13
4.9 Screening of commercial blends and base-oil substitution 14
4.10 Three-dimensional identity mapping 14
5. Critical Assessment and Limitations **15**
6. Conclusions and Recommendations **16**
References **16**
Summary **20**

1. Introduction

1.1 Economically motivated adulteration of edible oils

Edible oils occupy a position in the global food economy that renders them persistently attractive targets for economically motivated adulteration. High-value oils that command a price premium on the basis of botanical origin, extraction method, or health positioning are readily diluted with cheaper commodity oils whose bulk physical appearance, viscosity, and color are difficult to distinguish by eye. Extra virgin olive oil has been the archetypal case for decades, and a substantial analytical literature has grown around the detection of its adulteration with refined olive, hazelnut, and seed oils [15, 16, 17, 18, 19, 43, 44]. Avocado oil has more recently emerged as a comparably vulnerable commodity: surveys of retail product have reported that a large fraction of samples labeled as pure or extra virgin avocado oil are either oxidized or adulterated with lower-cost oils, a finding that has motivated the development of rapid authentication tools specific to that matrix [28, 29, 30]. The economic incentive is straightforward, since the wholesale differential between avocado or olive oil and canola, soybean, sunflower, or palm oil is frequently a factor of several, and partial substitution at the ten to forty percent level is both profitable and, without a molecular assay, effectively invisible.

The analytical response to this problem has traditionally rested on gas chromatography of fatty acid methyl esters, supplemented by the determination of sterols, tocopherols, and, in the case of olive and avocado oils, squalene. These methods are authoritative but require derivatization, are comparatively slow, and consume the sample. A complementary demand therefore exists for a rapid, non-destructive, and information-rich screening technique that can be applied to whole oil with minimal preparation, that reports simultaneously on many compositional axes, and whose output is amenable to the multivariate treatment on which modern authenticity decisions increasingly depend.

1.2 The molecular basis of the oil fingerprint

An edible oil is, to a first approximation, a mixture of triacylglycerols, each consisting of a glycerol backbone esterified at its three hydroxyl positions with fatty acyl chains. The identity of an oil is therefore governed by the statistical distribution of those acyl chains, which differ principally in length and in the number and position of carbon–carbon double bonds. Four chains dominate the common vegetable oils: the saturated palmitic (16:0) and stearic (18:0) acids, the monounsaturated oleic acid (18:1 cis-9), the diunsaturated linoleic acid (18:2 cis-9,12), and the triunsaturated α-linolenic acid (18:3 cis-9,12,15). The proportions in which these chains occur define both the nutritional character of an oil and its botanical signature; olive and avocado oils are oleic-dominant, sunflower and safflower oils occur in linoleic and high-oleic cultivars, soybean and corn oils are linoleic-rich, canola oil is distinguished by an appreciable linolenic content, and flaxseed oil is extraordinarily rich in linolenic acid, while coconut and palm oils and the animal fats are dominated by saturated chains. Because each of these structural features carries a characteristic ensemble of hydrogen environments, the acyl-chain distribution is transcribed with high fidelity into the ^{1}H NMR spectrum.

1.3 ^{1}H NMR as a rapid fingerprint of acyl-chain composition

High-resolution ^{1}H NMR spectroscopy has been applied to edible oils since the late 1990s, and the assignment of the proton resonances of triacylglycerols is now firmly established [1, 2, 3, 4, 12, 42]. The technique offers several practical advantages for authentication work. A spectrum is acquired in minutes on a simple solution of the neat oil in deuterated chloroform, without any chemical modification of the analyte, and the resulting integral pattern reports simultaneously on total unsaturation, on the balance between mono- and polyunsaturation, on the specific presence of linolenic chains, and on the saturated fraction. Methodologies for extracting the full fatty-acid profile from a single proton spectrum have been described and refined by several groups [2, 5, 6, 7, 8], and the same spectra have been shown to support the determination of iodine value [1, 2] and, through multivariate treatment, the classification of botanical origin and the detection of adulteration [16, 17, 26, 40, 41, 43]. The maturation of low-field benchtop instrumentation has further widened the applicability of the approach, since even spectrometers operating at 40 to 60 MHz retain sufficient resolution to separate the diagnostic olefinic, bis-allylic, and terminal-methyl regions used here [29, 35, 30].

1.4 Scope and objectives

The present work treats a large internal library of retail-oil ^{1}H NMR spectra as a single combinatorial dataset and asks, systematically rather than anecdotally, which arithmetic combinations of the ten integrated regions carry the most authentication value. Three objectives are pursued in turn. First, the per-triacylglycerol normalization is exploited to convert the raw integrals into a complete molar fatty-acid accounting and an iodine value, and these derived quantities are validated against the compositional literature. Second, every single integral, every pairwise ratio, and a set of chemically motivated composite expressions are screened for their power to discriminate among botanical classes and to quantify deliberate adulteration, and the best combinations are displayed as two- and three-dimensional identity maps. Third, gravimetrically defined mixtures of avocado oil with canola, soybean, and palm oils are used to construct quantitative calibrations and to establish detection limits, and the resulting coordinate system is applied to the screening of commercial blends. Throughout, the boundaries of what the ten-region fingerprint can and cannot establish are stated explicitly, so that the method may be deployed with an accurate sense of its evidentiary weight.

2. Quality and Authenticity Parameters Accessible by ^{1}H NMR

2.1 The ten diagnostic regions of the edible-oil ^{1}H NMR spectrum

The ^{1}H NMR spectrum of a triacylglycerol dissolved in deuterated chloroform distributes its intensity across a compact set of well-separated regions, each associated with a specific hydrogen environment on the glycerol backbone or the acyl chains. In the present dataset these have been integrated as ten regions, labeled A through J from high to low field, whose chemical-shift limits and assignments are collected in Table 1 and displayed schematically in Figure 1. The olefinic protons of every carbon–carbon double bond resonate near 5.3 ppm and are captured principally in region J, with a minor contribution to region I that also contains the single glyceryl methine proton. The four glyceryl methylene protons of the sn-1 and sn-3 positions appear as the two characteristic doublets of doublets between 4.07 and 4.36 ppm and constitute region H. The bis-

allylic (doubly allylic) methylene protons situated between two double bonds, which are the structural hallmark of polyunsaturation, resonate between 2.7 and 2.9 ppm and are here resolved into region G1, weighted toward the linolenic environment, and region G2, weighted toward the linoleic environment. The α-methylene protons adjacent to the ester carbonyls constitute region F near 2.3 ppm, the allylic methylene protons flanking the double bonds give regions E1 and E2 between 1.94 and 2.14 ppm, the β-methylene protons form region D near 1.6 ppm, the large bulk-methylene envelope is divided into regions C1 and C2 between 1.16 and 1.46 ppm, and the terminal methyl protons furnish region B, specific to the ω-3 (linolenic) chains near 0.97 ppm, and region A, comprising the methyl protons of all other chains near 0.88 ppm [1, 2, 3, 4, 5, 42].

Figure 1. Assignment of the ten integrated ¹H NMR regions (A-J) of edible-oil triacylglycerols (CDCl₃; intensities normalized to the glyceryl CH₂ signal H = 100, i.e. 4 protons per triacylglycerol)

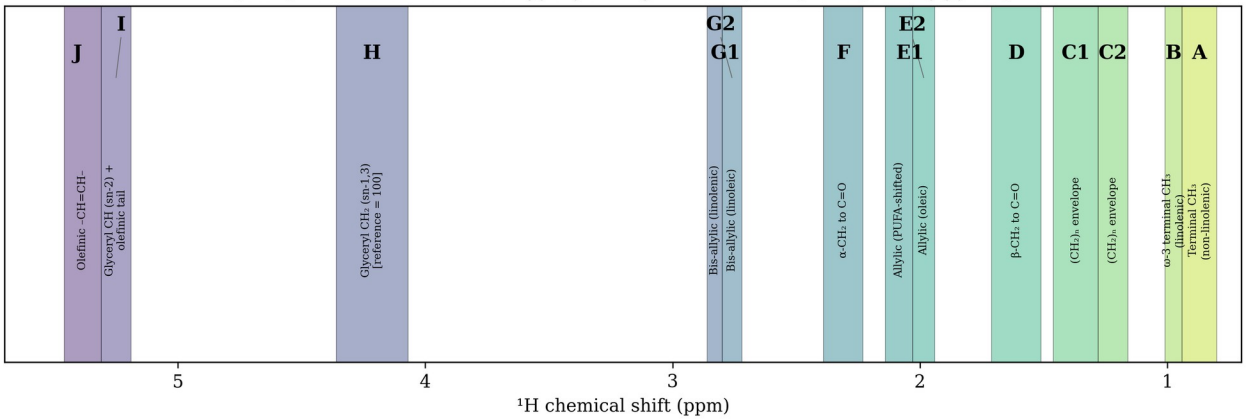

Figure 1. Schematic assignment of the ten integrated ¹H NMR regions (A–J) of edible-oil triacylglycerols in $CDCl_3$. Intensities throughout this work are normalized to the glyceryl methylene signal H, which corresponds to exactly four protons per triacylglycerol and is set to 100; one proton per triacylglycerol therefore corresponds to 25 normalized units.

Table 1. Chemical-shift limits, assignments, and diagnostic role of the integrated regions

Region	δ (ppm)	Assignment	Protons / TAG	Principal diagnostic role
J	5.46–5.31	Olefinic –CH=CH–	2 per C=C	Total unsaturation
I	5.31–5.19	Glyceryl CH (sn-2) + olefinic tail	1 (+ olefinic)	Backbone reference / unsaturation
H	4.36–4.07	Glyceryl CH_2 (sn-1,3)	4 (≡100)	Per-TAG normalization anchor
G1	2.86–2.80	Bis-allylic CH_2 (linolenic-weighted)	4 per 18:3	Linolenic / ω-3 marker
G2	2.80–2.72	Bis-allylic CH_2 (linoleic-weighted)	2 per 18:2	Linoleic / polyunsaturation
F	2.39–2.23	α-CH_2 to carbonyl	6	Internal reference (3 chains)
E1	2.14–2.03	Allylic CH_2 (PUFA-shifted)	—	Polyunsaturated allylic
E2	2.03–1.94	Allylic CH_2 (oleic)	—	Monounsaturated allylic
D	1.71–1.51	β-CH_2 to carbonyl	6	Chain-distribution reference
C1	1.46–1.28	Bulk $(CH_2)_n$ envelope	—	Mean chain length
C2	1.28–1.16	Bulk $(CH_2)_n$ envelope	—	Mean chain length
B	1.01–0.94	Terminal CH_3 of linolenic chains	3 per 18:3	Linolenic / ω-3 marker
A	0.94–0.80	Terminal CH_3 of non-linolenic chains	3 per other	Saturated + oleic + linoleic methyl

2.2 Per-triacylglycerol normalization and proton bookkeeping

The decision to normalize every spectrum to the glyceryl methylene integral, setting H equal to 100, is more consequential than a mere scaling convention. Because every intact triacylglycerol, irrespective of its acyl-chain composition, carries exactly four such glyceryl protons, the normalization places all remaining integrals on a rigorous per-molecule basis: one proton per triacylglycerol corresponds to precisely 25 normalized units. The internal consistency of the dataset can therefore be checked against exact proton counts. The two terminal-methyl regions should sum to nine protons per triacylglycerol, since three chains each contribute a methyl group, and the observed mean of A plus B across the olive samples, close to 226 units, matches the expected 225 to within one percent. The α-methylene region F should correspond to six protons and is observed near 152 units against an expected 150. These identities confirm that the integration is quantitatively faithful and that the derived molar quantities developed below rest on a sound footing rather than on empirical calibration alone.

2.3 Recovery of molar fatty-acid composition

From the per-triacylglycerol integrals the molar composition of the acyl pool follows by direct proton counting. The number of linolenic chains per triacylglycerol is obtained from the ω-3 terminal-methyl region as B divided by seventy-five, since each linolenic chain contributes three protons scaled by twenty-five units. The number of unsaturated chains follows from the allylic regions, because each double-bond-bearing chain contributes four allylic protons regardless of whether it is mono-, di-, or triunsaturated, so that the sum of E1 and E2 divided by one hundred yields the unsaturated-chain count and, by difference from three, the saturated-chain count. The bis-allylic regions provide the polyunsaturated content, since the sum of G1 and G2 divided by twenty-five equals twice the number of linoleic chains plus four times the number of linolenic chains; the linoleic count is thereby recovered once the linolenic count is known, and the oleic (monounsaturated) count follows as the residual of the unsaturated chains after the polyunsaturated chains are removed. Expressed as mole percentages of the three acyl positions, these relations furnish the saturated, oleic, linoleic, and linolenic fractions reported throughout Section 4. The splitting of the allylic envelope into a polyunsaturation-shifted region E1 and an oleic region E2 provides an independent, and as shown below a highly discriminating, measure of the balance between mono- and polyunsaturation.

2.4 Iodine value and mean unsaturation

The mean number of carbon–carbon double bonds per triacylglycerol is obtained from the olefinic intensity as the sum of J and the olefinic portion of I, the latter recovered by subtracting the single glyceryl methine proton, divided by fifty. From this quantity the iodine value, the classical index of unsaturation expressed as grams of iodine absorbed per hundred grams of oil, is calculated using the mean triacylglycerol molar mass implied by the derived fatty-acid distribution [1, 2]. The approach reproduces the accepted iodine values of the reference oils, as documented in Section 4, and provides a continuous quality axis along which oxidative stability and nutritional classification can be read directly from the proton spectrum.

2.5 Oil-specific marker chemistry

Three marker systems carry most of the botanical information in the fingerprint. The linolenic system, comprising the ω-3 terminal methyl in region B and the linolenic-weighted bis-allylic intensity in region

G1, cleanly separates the linolenic-bearing oils, chiefly canola, soybean, walnut, hemp, and flaxseed, from the oleic oils in which linolenic acid is nearly absent. The linoleic system, dominated by region G2 and by the total bis-allylic intensity, distinguishes the linoleic-rich commodity oils such as soybean, corn, sunflower of the classical cultivar, grapeseed, and safflower. The saturated system, read from the bulk-methylene ratio C2/C1 together with the low olefinic intensity, isolates the saturated fats. Because the oleic-dominant oils are impoverished in all three of these marker systems, their mutual discrimination is the central analytical challenge of the dataset and is treated explicitly in Section 4.4.

3. Materials and Methods

3.1 Sample set and calibration mixtures

The dataset comprises 200 ¹H NMR spectra of retail edible oils, fats, and defined laboratory mixtures. The single-oil portion spans the oleic oils olive and avocado, which are the most heavily represented on account of their authentication interest, together with canola, soybean, corn, sunflower, safflower in both classical and high-oleic forms, grapeseed, walnut, hazelnut, almond, peanut, sesame, pumpkin-seed, hemp-seed, and flaxseed oils, the saturated coconut and palm oils, and a group of rendered animal fats including beef and bison tallow, pork lard, duck and chicken fat, wild boar fat, and lamb tallow. The defined mixtures consist of three gravimetric spiking series in which a single avocado oil was blended with increasing volume fractions of canola, soybean, or palm oil at nominal levels of five, ten, twenty, forty, and sixty percent, the palm series being extended to one hundred percent, together with a set of commercial "canola and olive oil" blends of independent provenance. Because the densities of these oils lie within a narrow band close to 0.91 to 0.92 grams per milliliter, the volumetric spike levels correspond to mass fractions to within one to two percent, and this small distinction is carried forward in the interpretation of the calibrations.

All spectra were acquired on neat oil dissolved in deuterated chloroform under the standard conditions used in the laboratory for triacylglycerol analysis, and the ten regions were integrated according to the limits of Table 1. The reported figures were obtained from the normalized integral table; no spectrum was reprocessed for the present study, so that the analysis reflects the reproducibility of the routine method as practiced.

3.2 Data extraction, normalization, and quality control

Each spectrum contributes a vector of thirteen normalized integrals, obtained by interpreting the regions in the order A, B, C2, C1, D, E2, E1, F, G2, G1, H, I, J and scaling every value by the factor that sets H to 100. A single record carrying a non-numeric entry was removed, leaving two hundred complete vectors. Botanical classes were assigned from the sample descriptions, and a small number of records required adjudication where an internal identifier and a text description disagreed. The most consequential such case concerned a spiking series whose sample identifiers designated a canola adulterant while the accompanying descriptions read "soybean." The conflict was resolved on spectroscopic rather than clerical grounds. Across the five to sixty percent range the identifier-designated canola series exhibited only a modest rise in the linoleic-weighted region G2, from 21.7 to 29.9 units, while retaining a high linolenic-to-linoleic ratio G1/G2 near 0.33; the separately labeled soybean series, by contrast, showed region G2 rising steeply from 24.1 to 58.2 units with a lower ratio near 0.21. Since canola oil is oleic-dominant with a comparatively high

linolenic-to-linoleic ratio whereas soybean oil is strongly linoleic, and since the two trajectories extrapolate respectively toward the pure-canola and pure-soybean end-member intensities, the identifier assignment was judged correct and the descriptions were treated as the erroneous field. This determination is documented here because it materially affects the interpretation of the canola calibration and illustrates the self-checking capacity of the fingerprint.

3.3 Derived-parameter computation

The molar fatty-acid fractions, mean double-bond number, and iodine value were computed for every spectrum according to the proton-counting relations of Section 2, using acyl molar masses of 270, 282.46, 280.45, and 278.43 grams per mole for the saturated, oleic, linoleic, and linolenic pools respectively, and a triacylglycerol molar mass obtained from the composition-weighted acyl mass and the glycerol backbone. For the near-saturated coconut and palm samples, in which the polyunsaturated intensity approaches the noise floor, the linoleic estimate occasionally returns a small negative value; such cases were floored at zero and are flagged in the interpretation, since the molar model is constructed for unsaturated oils and is not intended for quantitative fatty-acid work on the saturated fats.

3.4 Combinatorial screening

A feature library of one hundred fifty-seven expressions was constructed from the twelve compositional integrals, comprising the individual integrals, all ordered pairwise ratios, and a curated set of chemically motivated composites including the total bis-allylic intensity, the total allylic intensity, the olefinic intensity, the linolenic methyl fraction B/(A+B), the ratio G1/G2, the bulk-methylene ratio C2/C1, and several intensities referenced to the α-methylene signal F. Each expression was evaluated against two objectives. Discriminating power among the six best-populated single-oil classes was quantified by the one-way analysis-of-variance F statistic, and the separation of the difficult avocado–olive pair was quantified separately by the standardized mean difference. Quantitative response to adulteration was assessed by linear regression of each expression against the known spike level within each series, with ranking by the coefficient of determination and by the detection limit, the latter estimated as three times the residual standard deviation divided by the absolute slope.

3.5 Multivariate analysis

Principal-component analysis was performed on the twelve autoscaled compositional integrals across all two hundred spectra. Supervised classification was assessed by linear discriminant analysis restricted to the 148 single-oil spectra of the eight classes for which at least three replicates were available, with performance estimated by leave-one-out cross-validation so that no sample contributed to the model under which it was classified. The same cross-validation protocol was applied to the targeted avocado–olive problem using compact combinations of the top-ranked ratios.

4. Results and Discussion

4.1 Molar fatty-acid profiles and iodine values

The molar fatty-acid fractions recovered from the proton bookkeeping are collected in Table 2 and displayed in Figures 2 and 3. The agreement with the compositional literature is close across the full range of oil types and provides the primary validation of the per-triacylglycerol model. The oleic oils olive and avocado return oleic fractions of 72 and 68 mole percent with low polyunsaturation, canola returns 58 percent oleic with 22 percent linoleic and an appreciable 10 percent linolenic, soybean and corn are correctly rendered as linoleic-dominant near 47 percent, and flaxseed is placed at 54 percent linolenic. The saturated fats are resolved at the opposite extreme, coconut returning a 95 percent saturated fraction and an iodine value near 5, and the animal fats clustering near 45 percent saturated. The derived iodine values, spanning from coconut through the oleic oils near 82 to 89, the linoleic oils near 120 to 130, and flaxseed at 182, reproduce the accepted ranges and establish that a single proton spectrum suffices to place any of these oils on the classical unsaturation scale [1, 2, 5].

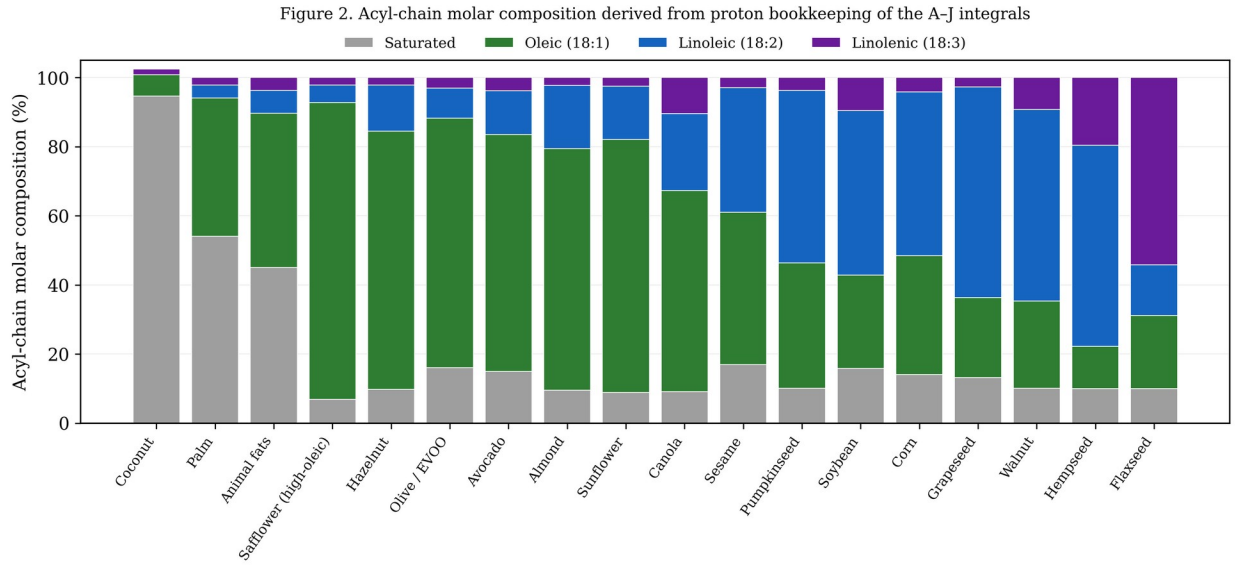

Figure 2. Acyl-chain molar composition (saturated, oleic, linoleic, and linolenic) recovered from the A–J proton bookkeeping, ordered from the most saturated to the most polyunsaturated oils. The progression from coconut and palm through the oleic oils to the linolenic-rich flaxseed is continuous and quantitative.

Figure 3. Iodine value estimated from olefinic proton content (J + I) per triacylglycerol

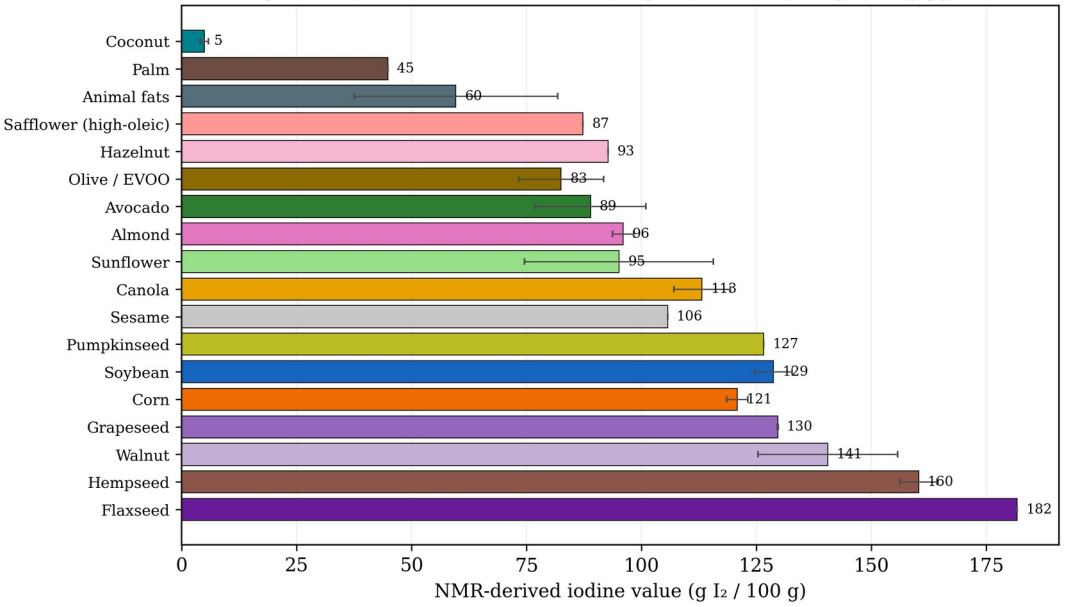

Figure 3. NMR-derived iodine value by oil class, estimated from the olefinic proton content per triacylglycerol. Error bars denote one standard deviation within each class. The values reproduce the accepted iodine-value ranges, from coconut near 5 to flaxseed near 182.

Table 2. NMR-derived molar composition, iodine value, and key diagnostic ratios by oil class

Oil class	n	Sat %	Oleic %	Lin %	Lnn %	C=C/TAG	Iodine	G1/ G2	C2/C1
Olive / EVOO	53	16.1	72.1	8.7	3.1	2.86	83	0.17	0.905
Avocado	65	15	68.5	12.7	3.9	3.08	89	0.14	0.808
Canola	9	9.1	58.3	22.2	10.4	3.92	113	0.371	0.636
Soybean	3	15.8	27.1	47.5	9.6	4.44	129	0.219	0.579
Corn	4	14.1	34.4	47.3	4.2	4.17	121	0.072	0.564
Sunflower	7	8.9	73.2	15.4	2.6	3.3	95	0.087	0.712
Safflower	1	11.6	32.3	53.4	2.8	4.36	126	0.045	0.499
Safflower (high-oleic)	1	6.9	85.8	5.1	2.1	3.03	87	0.068	0.745
Grapeseed	2	13.2	23.1	61	2.7	4.48	130	0.049	0.441
Walnut	2	10.1	25.3	55.4	9.3	4.86	141	0.196	0.422
Hempseed	2	10	12.2	58.1	19.6	5.53	160	0.493	0.41
Flaxseed	1	10	21.1	14.7	54.2	6.26	182	1.494	0.451
Almond	2	9.5	69.9	18.2	2.3	3.33	96	0.051	0.681
Hazelnut	1	9.8	74.6	13.3	2.2	3.22	93	0.057	0.735
Sesame	1	16.9	44.1	36	3	3.65	106	0.058	0.7
Pumpkinseed	1	10.1	36.3	50	3.7	4.38	127	0.068	0.482
Coconut	3	94.6	6.2	0	1.7	0.17	5	0.054	2.604
Palm	1	54.1	40	3.7	2.2	1.53	45	0.073	1.772
Animal fats (tallow/lard)	7	45	44.7	6.6	3.8	2.04	60	0.557	1.718

Values are class means. Saturated, oleic, linoleic (Lin), and linolenic (Lnn) fractions are mole percentages of the acyl pool; the small nonzero linolenic values for oils containing essentially no 18:3 reflect the additive baseline discussed in Section 5. Iodine value is expressed as grams I_2 per 100 g.

4.2 Correlation structure of the integrals

Before the discriminating combinations are examined individually, the correlation structure of the twelve integrals across the whole dataset, shown in Figure 14, clarifies why ratios rather than single integrals carry the authentication information. The unsaturation-associated regions J, I, E1, G1, and G2 are strongly and positively intercorrelated, as are the terminal-methyl region A and the bulk-methylene region C2 among the saturated environments, while the two families are mutually anticorrelated. This collinearity is the spectroscopic expression of the underlying compositional constraint that the acyl pool is a closed system, and it implies that a well-chosen ratio, which cancels the shared per-triacylglycerol scaling and isolates a single compositional contrast, will generally outperform any raw integral as a classifier.

Figure 14. Correlation structure of the twelve A–J integrals across all samples

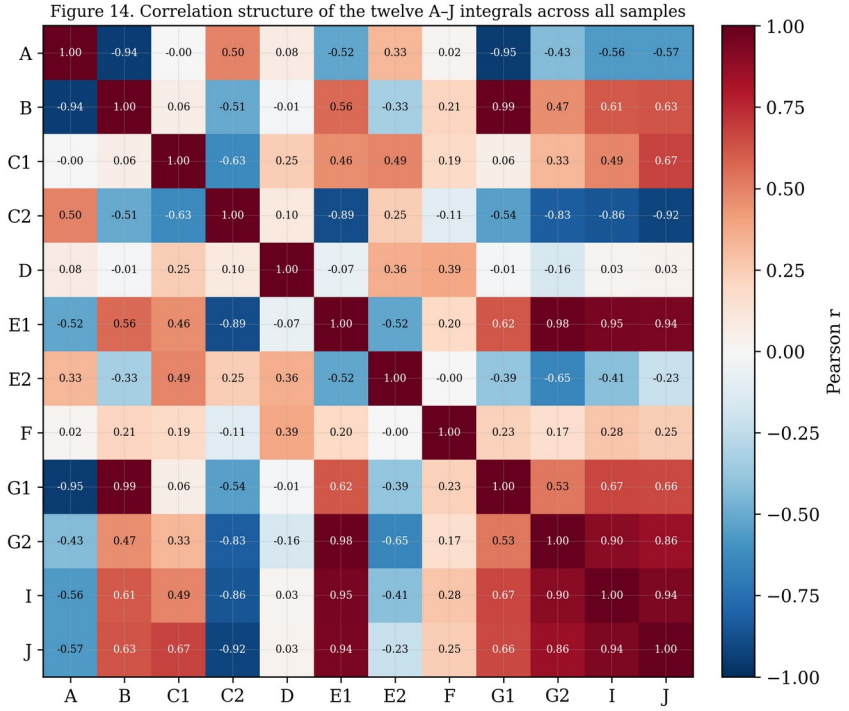

Figure 14. Pearson correlation matrix of the twelve compositional integrals across all two hundred spectra. The block of positively correlated unsaturation markers (J, I, E1, G1, G2, B) and its anticorrelation with the saturated-environment markers (A, C2) reflect the closed-system constraint on acyl composition.

4.3 The master identity maps

The most compact global summary of the dataset is obtained by plotting the linolenic marker against the polyunsaturation load, as in Figure 4, where the abscissa is the ω-3 methyl fraction B/(A+B) and the ordinate is the total bis-allylic intensity referenced to the α-methylene signal. In this plane the oils order themselves along two nearly orthogonal chemical axes. Movement to the right tracks increasing linolenic content and carries the oil classes from the oleic oils at the origin, through canola and the nut oils, to flaxseed

at the far margin; movement upward tracks total polyunsaturation and separates the linoleic-rich soybean, corn, sunflower, grapeseed, and safflower oils from the oleic oils below. The complementary fatty-acid map of Figure 5, in which molar oleic content is plotted against total polyunsaturation, presents the same information in the more familiar compositional coordinates and confirms the placement of every class. Together these maps constitute the identity atlas against which an unknown oil, or a suspected blend, may be located at a glance.

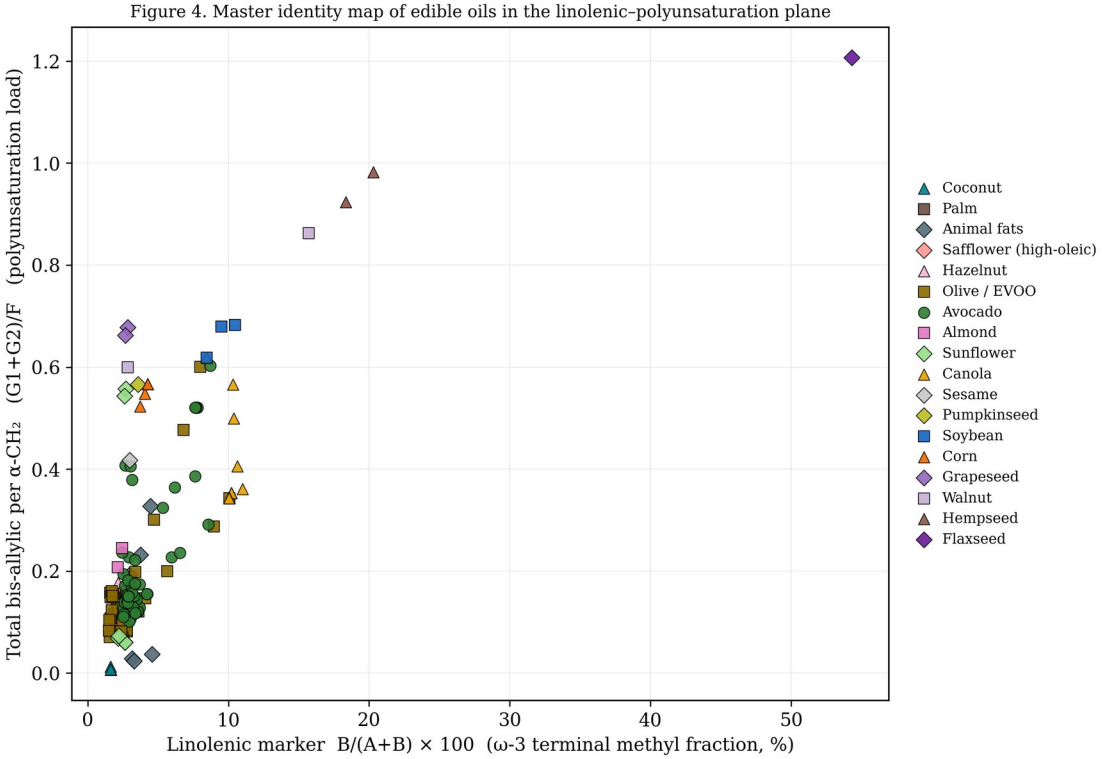

Figure 4. Master identity map of the edible oils in the linolenic–polyunsaturation plane. The abscissa B/(A+B) measures the ω-3 terminal-methyl fraction and the ordinate (G1+G2)/F measures total bis-allylic intensity per α-methylene proton. The two axes resolve the oleic oils (lower left), the linoleic oils (upper left), the linolenic oils (right), and the saturated fats (origin).

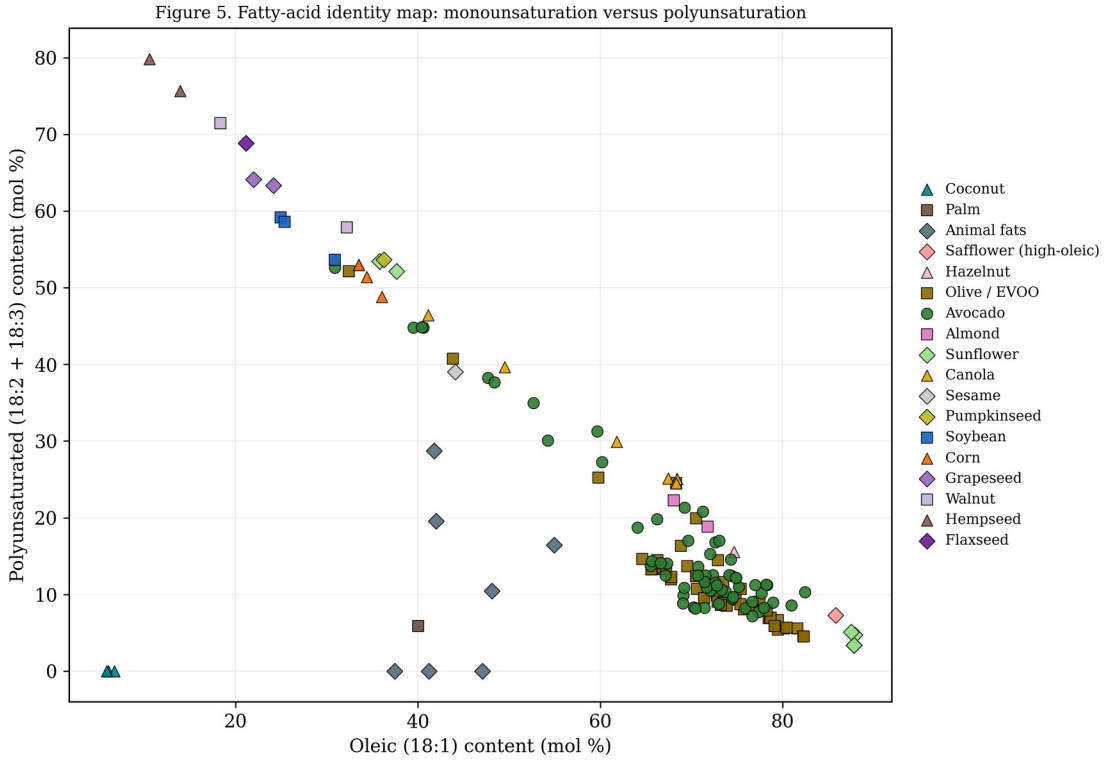

Figure 5. Fatty-acid identity map of molar oleic content against total polyunsaturated (18:2 + 18:3) content, derived from the proton bookkeeping. The strong anticorrelation defines the compositional backbone along which the common vegetable oils are distributed.

4.4 Separation of the high-oleic oils and the avocado–olive problem

The oleic oils present the hardest discrimination problem in the dataset, because avocado, olive, high-oleic safflower, high-oleic sunflower, almond, hazelnut, and peanut oils share oleic fractions in the range of roughly 68 to 86 mole percent and are therefore nearly coincident on any map whose axes are dominated by unsaturation. It is a notable and honestly acknowledged feature of these data that the several "sunflower" samples returned oleic contents near 73 percent, identifying them as high-oleic cultivars rather than the classical linoleic type, so that they overlap the avocado region and cannot be assumed to occupy the linoleic domain. Within this crowded oleic group the discriminating information resides not in unsaturation but in the finer features of the methylene distribution and the olefinic multiplet. Figure 6 plots the chain-distribution ratio D/C1, the ratio of β-methylene to bulk methylene, against the olefinic fine-structure ratio I/J, and shows that avocado and olive, while overlapping, occupy statistically distinct regions. A single ratio, D/C1, classifies the two oils at 88.7% under leave-one-out cross-validation, and a compact three-ratio linear-discriminant model combining D/C1, C2/C1, and I/J raises that figure to 93.0%. The separation is genuine and useful for screening, but it is not absolute, and the residual overlap is the subject of the candid assessment in Section 5.

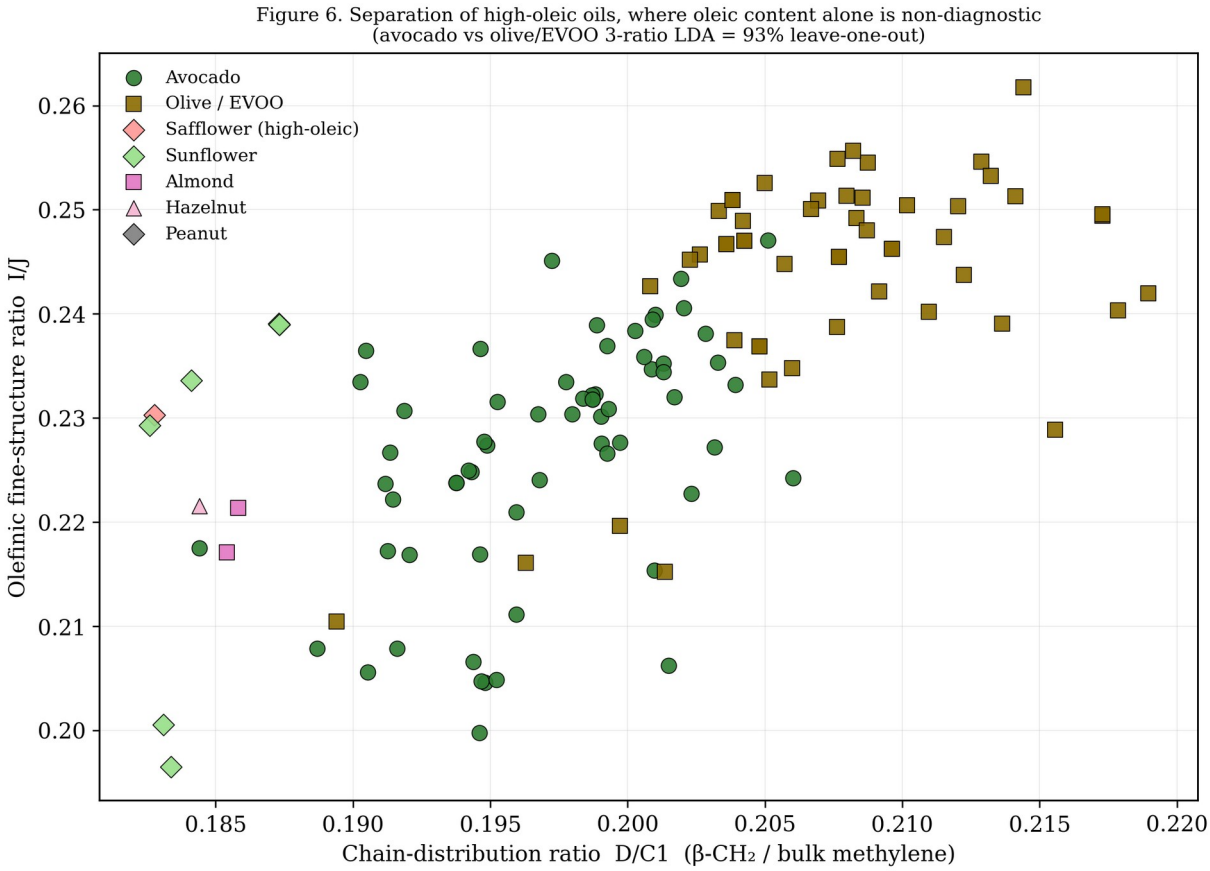

Figure 6. Separation of the high-oleic oils, for which oleic content itself is non-diagnostic, in the plane of the chain-distribution ratio D/C1 and the olefinic fine-structure ratio I/J. Avocado and olive occupy overlapping but statistically distinct regions; a three-ratio model (D/C1, C2/C1, I/J) classifies the pair at 93% under leave-one-out cross-validation.

4.5 Principal-component structure of the fingerprint

Principal-component analysis of the autoscaled twelve-integral fingerprint condenses the dataset without supervision and confirms the chemical picture developed above. The first three components account for 54.4, 17.7, and 12.8 percent of the total variance respectively, or 84.9 percent in aggregate. The first component loads positively on the unsaturation and polyunsaturation markers B, E1, G1, G2, I, and J and negatively on the saturated-environment markers A and C2, and is therefore correctly read as an unsaturation axis; the second component, loading on the bulk-methylene region C1 and the oleic-allylic region E2, expresses chain length and monounsaturation. The scores map of Figure 7 reproduces the identity atlas of Figure 4 in the unsupervised coordinates, placing the saturated fats, the oleic oils, the linoleic oils, and flaxseed in mutually distinct regions, while the loadings of Figure 8 make explicit which integrals drive each direction. The concordance between the supervised and unsupervised views indicates that the structure recovered here is intrinsic to the data and not an artifact of the class labels.

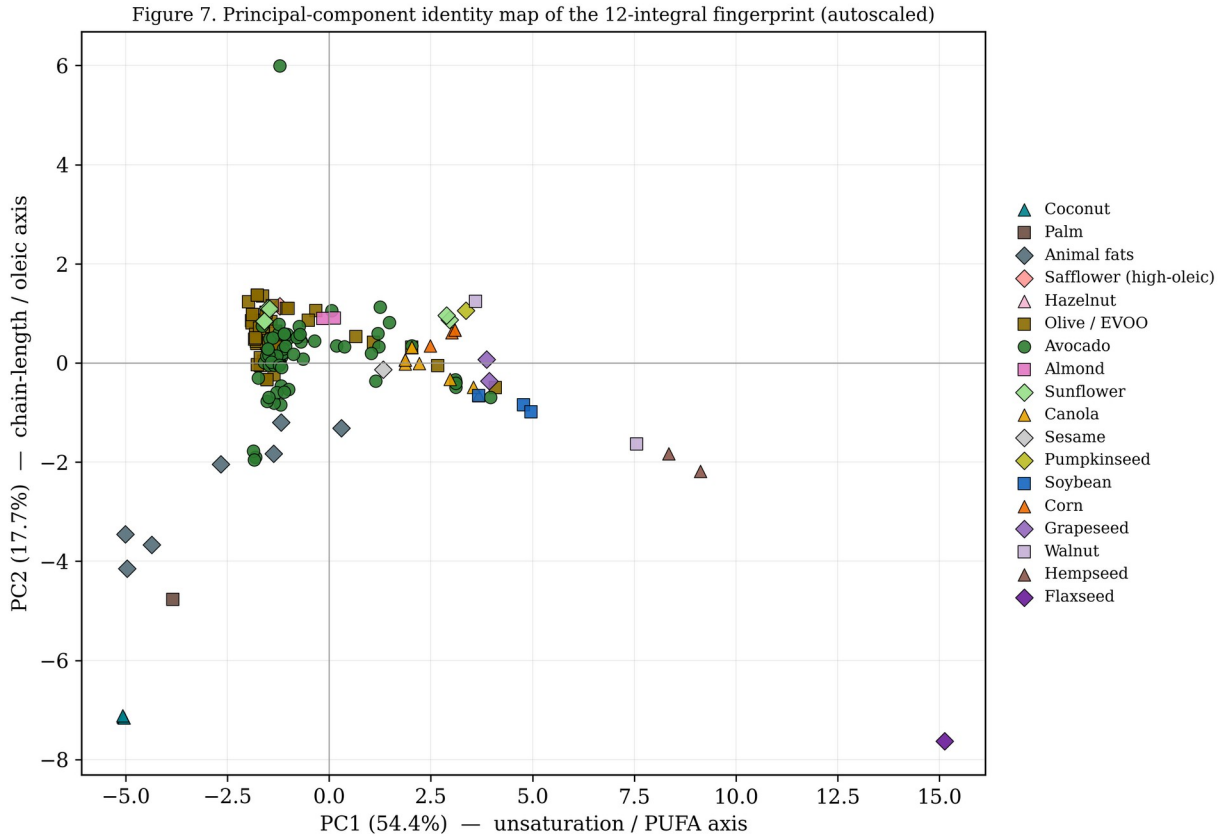

Figure 7. Principal-component scores map of the twelve-integral fingerprint (autoscaled, all spectra). PC1 (54.4% of variance) is an unsaturation axis and PC2 (17.7%) a chain-length axis; the classes separate along the same chemical directions recovered by the ratio maps.

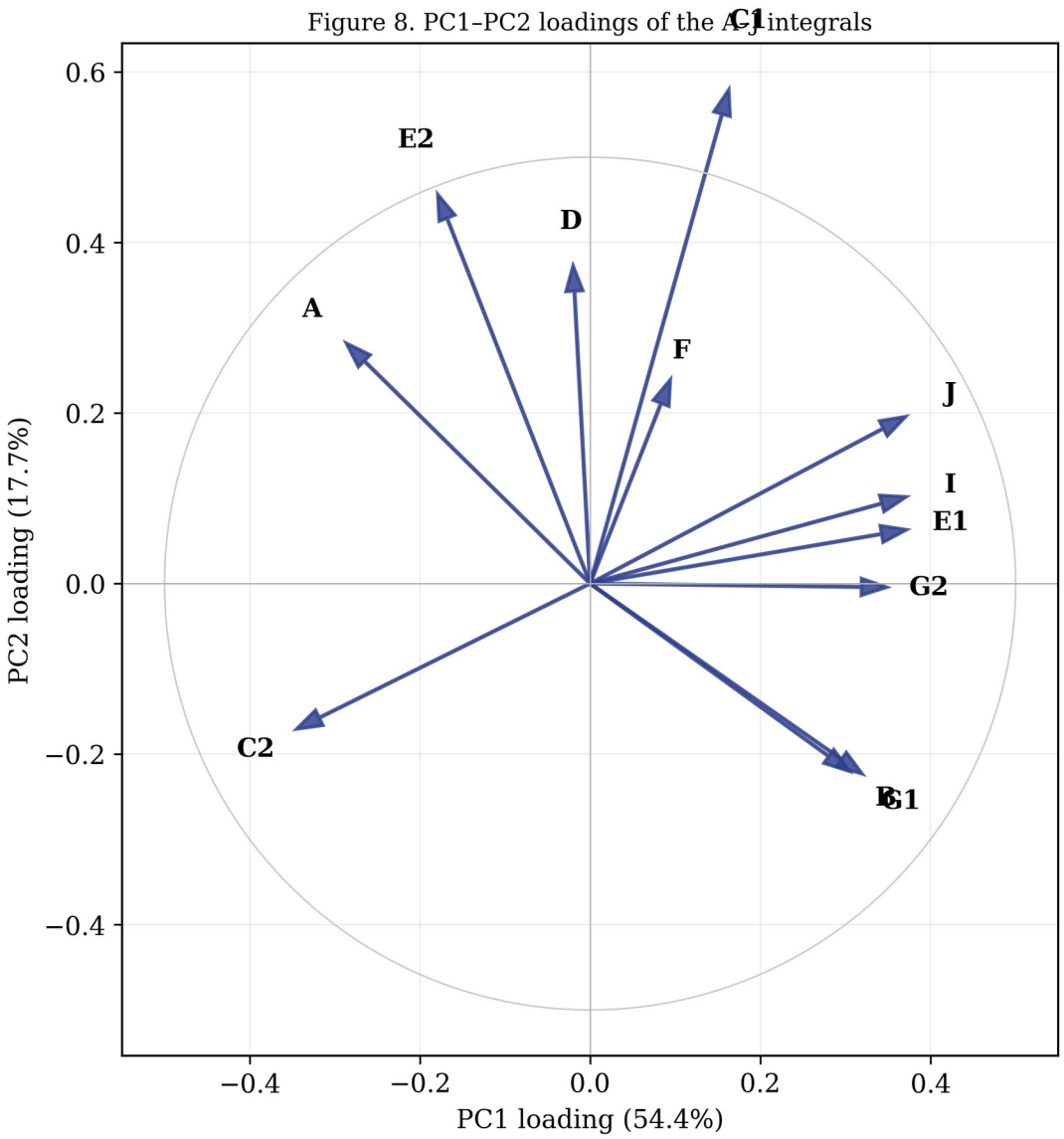

Figure 8. PC1–PC2 loadings of the A–J integrals. The unsaturation markers (J, I, G1, G2, B, E1) load together and oppose the saturated-environment markers (A, C2), while C1, D, and E2 define the orthogonal chain-length axis.

4.6 Combinatorial ranking of diagnostic combinations

The systematic screen identifies the arithmetic combinations that carry the greatest discriminating power among the botanical classes, and the leading expressions are collected in Table 3. Three families dominate the ranking. The linolenic family, represented by the region B itself and by its ratios to the reference and saturated regions such as B/I, B/A, and B/(A+B), and by the linolenic bis-allylic ratios G1/I and G1/A, achieves the highest F statistics because linolenic content is the single most botanically informative axis in the common oils. The chain-distribution family, represented by C1/D and by the olefinic ratio J/I, ranks equally highly and supplies precisely the information required to separate the oleic oils that the linolenic markers cannot distinguish. The interpretation is chemically transparent: where an unknown oil registers a low value on every linolenic and polyunsaturation ratio, it belongs to the oleic group, and its identity within

that group is then resolved by the chain-distribution and olefinic-fine-structure ratios. This hierarchical logic, rather than any single master parameter, is the practical output of the combinatorial analysis.

Table 3. Leading integral combinations for discrimination among botanical classes

Combination	ANOVA F	Chemical interpretation
C1/D	52.7	Bulk-to-β methylene; mean chain length
J/I	52.4	Olefinic to backbone; total unsaturation
B/I	42.7	Linolenic methyl per backbone proton
B/C2	42.4	Linolenic methyl vs saturated methylene
G1/I	39.8	Linolenic bis-allylic per backbone
B/A	39.5	ω-3 vs non-ω-3 terminal methyl
G1/C2	39.0	Linolenic bis-allylic vs saturated methylene
B	38.4	Linolenic terminal methyl (absolute)
B/(A+B)	37.7	Linolenic mole fraction of methyl
G1/A	37.0	Linolenic bis-allylic vs total methyl

F statistics from one-way analysis of variance across the six best-populated single-oil classes (olive, avocado, canola, soybean, corn, sunflower). Reciprocal ratios have been consolidated. The linolenic (B, G1) and chain-distribution (C1/D, J/I) families dominate.

4.7 Adulteration drives distinct and interpretable vectors

When avocado oil is deliberately adulterated, the fingerprint does not merely shift in magnitude but moves in a direction characteristic of the adulterant, so that detection and identification are achieved simultaneously. Figure 9 plots the gravimetric spiking series in the plane of the linolenic-to-linoleic ratio G1/G2 and the polyunsaturation load, with the pure avocado base marked as a star. The three adulterants describe three clearly divergent trajectories. Canola, being oleic-dominant but comparatively rich in linolenic acid, carries the base to the right along the G1/G2 axis while raising the polyunsaturation load only moderately. Soybean, being strongly linoleic, drives the base steeply upward in polyunsaturation with a smaller lateral displacement. Palm, being saturated, moves the base downward as it dilutes the unsaturated intensity. The three-dimensional rendering of Figure 10, in the coordinates of the linolenic, linoleic, and olefinic intensities referenced to the α-methylene signal, resolves the trajectories still more completely and demonstrates that the direction of the displacement vector encodes the identity of the adulterant. This vectorial behavior is the central practical result of the study, because it converts a quantitative screening measurement into a qualitative identification of the substituting oil.

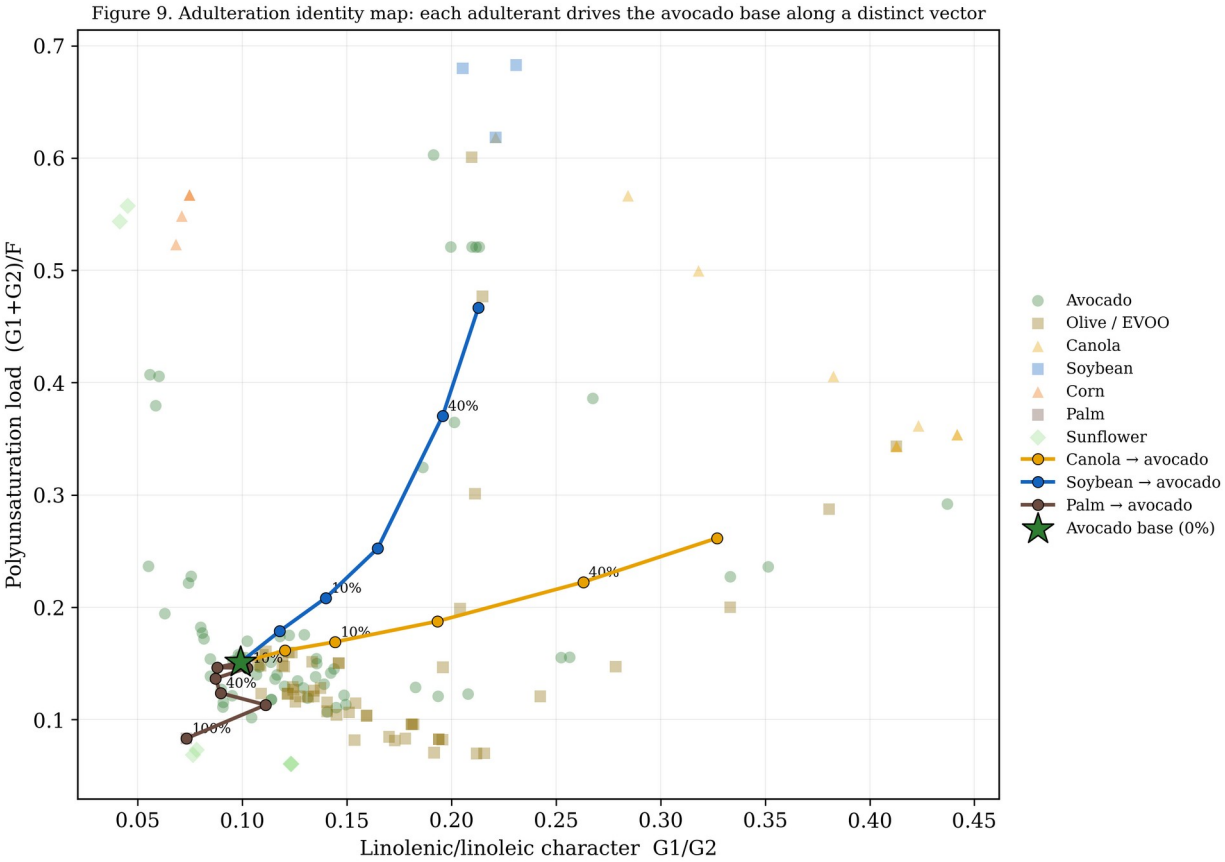

Figure 9. Adulteration identity map. Each adulterant drives the avocado base (star) along a distinct vector in the plane of the linolenic-to-linoleic ratio G1/G2 and the polyunsaturation load (G1+G2)/F: canola to the right, soybean steeply upward, palm downward. Faint symbols are the pure reference oils; several commercial avocado samples themselves fall well away from the base.

Figure 10. Three-dimensional adulteration trajectories in bis-allylic / olefinic space

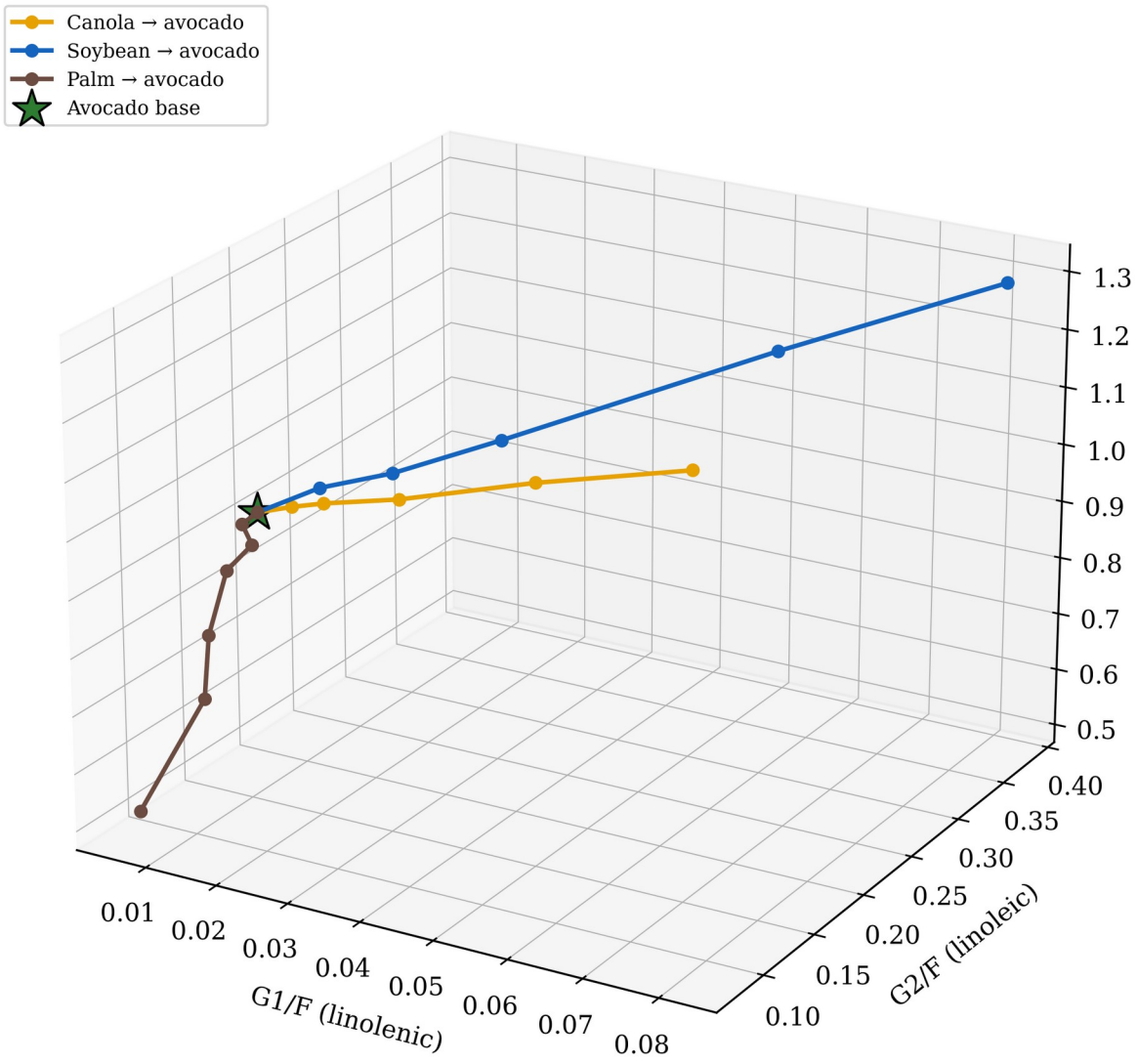

Figure 10. Three-dimensional adulteration trajectories in the coordinates of the linolenic (G1/F), linoleic (G2/F), and olefinic ((J+I−25)/F) intensities. The divergence of the canola, soybean, and palm paths from the common avocado origin encodes both the level and the identity of the adulterant.

4.8 Quantitative calibration and detection limits

Along each adulteration vector the response is strikingly linear, and the resulting calibrations, summarized in Table 4 and displayed in Figure 11, support quantification at low levels of substitution. For canola in avocado the polyunsaturation load (G1+G2)/F rises linearly with a coefficient of determination of 0.9995 and a detection limit of 1.6 volume percent, while the ratio G1/G2 provides an independent and mechanistically specific confirmation. For soybean in avocado the linolenic bis-allylic intensity G1 responds with a coefficient of determination of 0.9994 and a detection limit of 1.8 volume percent. For palm in avocado, where the adulterant dilutes rather than augments the unsaturation, the olefinic intensity

(J+I−25)/F falls linearly with a coefficient of determination of 0.9997 and a detection limit of 1.8 volume percent, and the linoleic intensity G2 furnishes an equivalent descending calibration. That detection limits between 1.6 and 2.3 volume percent are achieved across three chemically dissimilar adulterants, using integrals that require no more than the routine spectrum, establishes the quantitative credentials of the method for screening purposes. It should be emphasized that these calibrations are anchored on a single avocado base and defined against volumetric spikes, considerations that bound their transfer to independent matrices and are addressed in Section 5.

Figure 11. Adulteration calibration curves against gravimetric spike level (shared avocado base = 0%)

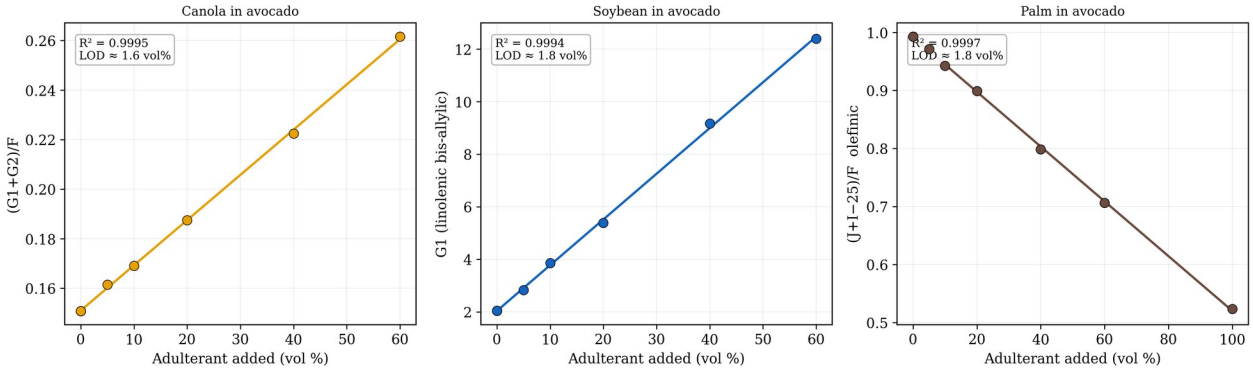

Figure 11. Adulteration calibration curves against gravimetric spike level, with the shared avocado base taken as the zero point. Canola and soybean raise their respective unsaturation markers; palm lowers the olefinic intensity. All three regressions exceed a coefficient of determination of 0.999, with detection limits below 1.9 volume percent.

Table 4. Adulteration calibrations and detection limits (avocado base = 0%)

Adulterant	Predictor	R²	Slope	LOD (vol %)	LOQ (vol %)
Canola	(G1+G2)/F	0.9995	0.0018	1.57	5.23
Canola	G1/G2	0.9939	0.0039	5.63	18.76
Soybean	G1 (18:3)	0.9994	0.174	1.77	5.9
Soybean	(G1+G2)/F	0.9990	0.0053	2.26	7.54
Palm	(J+I-25)/F	0.9997	-0.0047	1.79	5.98
Palm	G2 (18:2)	0.9998	-0.0938	1.66	5.52

Linear regressions of each predictor against known volumetric spike level. LOD and LOQ estimated as three and ten times the residual standard deviation divided by the absolute slope. Two predictors are reported per adulterant to show the primary marker and an independent confirmatory marker.

4.9 Screening of commercial blends and base-oil substitution

The coordinate system developed on the defined mixtures applies directly to commercial product of independent origin. Figure 13 places a set of retail blends marketed as mixtures of canola and olive oil onto

the adulteration map. Most fall, as their labeling implies, in the canola region at elevated G1/G2, consistent with a canola base carrying a minor olive fraction. One sample, however, is displaced to a markedly low G1/G2 accompanied by a high linoleic load, a position incompatible with a canola base and characteristic instead of a corn or soybean base. The linolenic markers thus expose a base-oil substitution that the product label does not disclose, precisely the kind of discrepancy that authentication analysis exists to detect. It is further notable, in Figure 9, that a number of the commercial avocado samples themselves lie well away from the pure-avocado base and toward the adulterant regions, consistent with the widely reported vulnerability of the retail avocado-oil category and indicating that the same screening coordinates flag suspect single-oil product as readily as declared blends [28, 30].

Figure 13. Screening commercial “canola + EVOO” blends: base-oil substitution is exposed by G1/G2

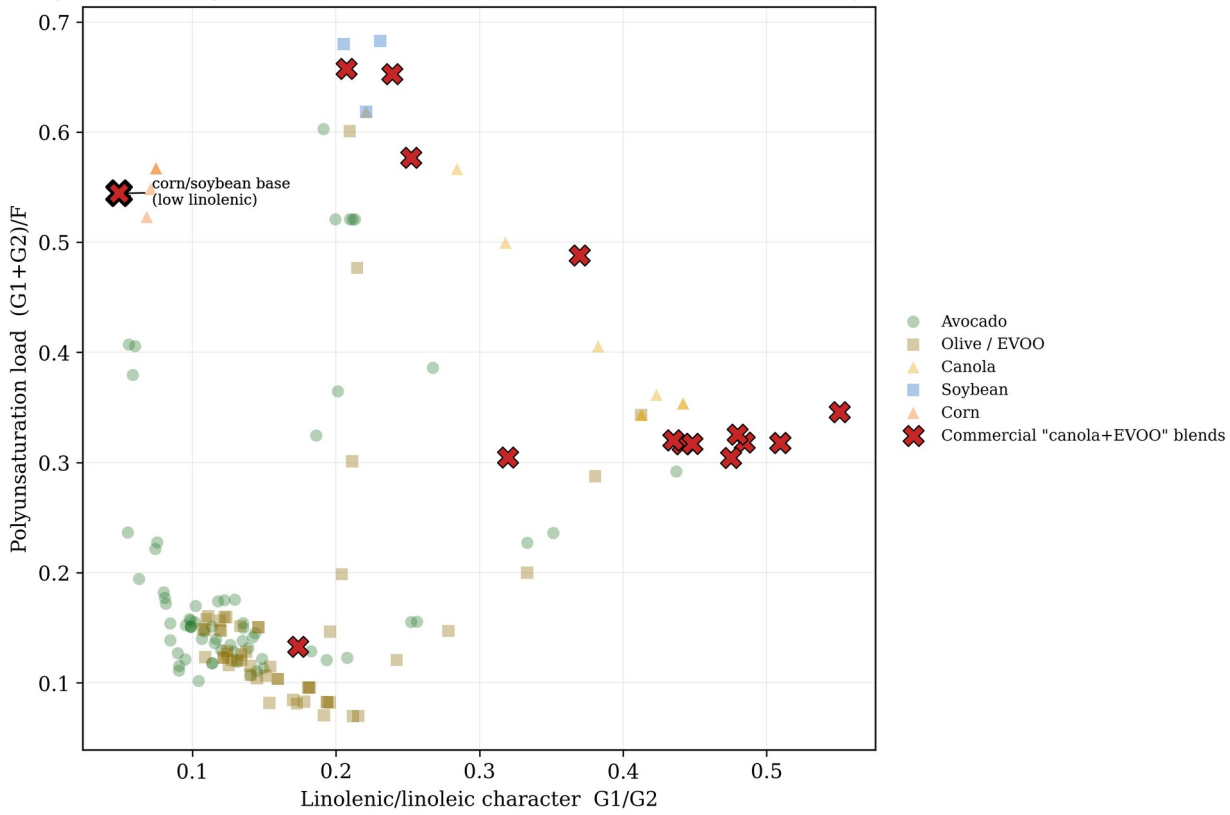

Figure 13. Screening of commercial "canola and olive oil" blends on the adulteration map. Most samples occupy the canola region, but one is displaced to low G1/G2 and high polyunsaturation, a signature of a corn- or soybean-type base rather than the declared canola, demonstrating detection of undisclosed base-oil substitution.

4.10 Three-dimensional identity mapping

Where the two-dimensional maps collapse classes that in fact differ along a third chemical axis, a three-dimensional projection restores the separation. Figure 12 combines the linolenic marker B/(A+B), the polyunsaturation load, and the bulk-methylene ratio C2/C1 into a single identity volume. The added methylene axis lifts the saturated fats, coconut, palm, and the animal fats, cleanly out of the plane occupied by the unsaturated oils, resolves flaxseed along the linolenic axis, and preserves the separation of the linoleic and oleic groups established in the planar maps. The three-dimensional map is offered as the most complete

single visualization of the identity landscape spanned by the ten-region fingerprint, within which any unknown oil can be situated relative to the full reference set.

Figure 12. Three-dimensional identity map (linolenic × polyunsaturation × methylene distribution)

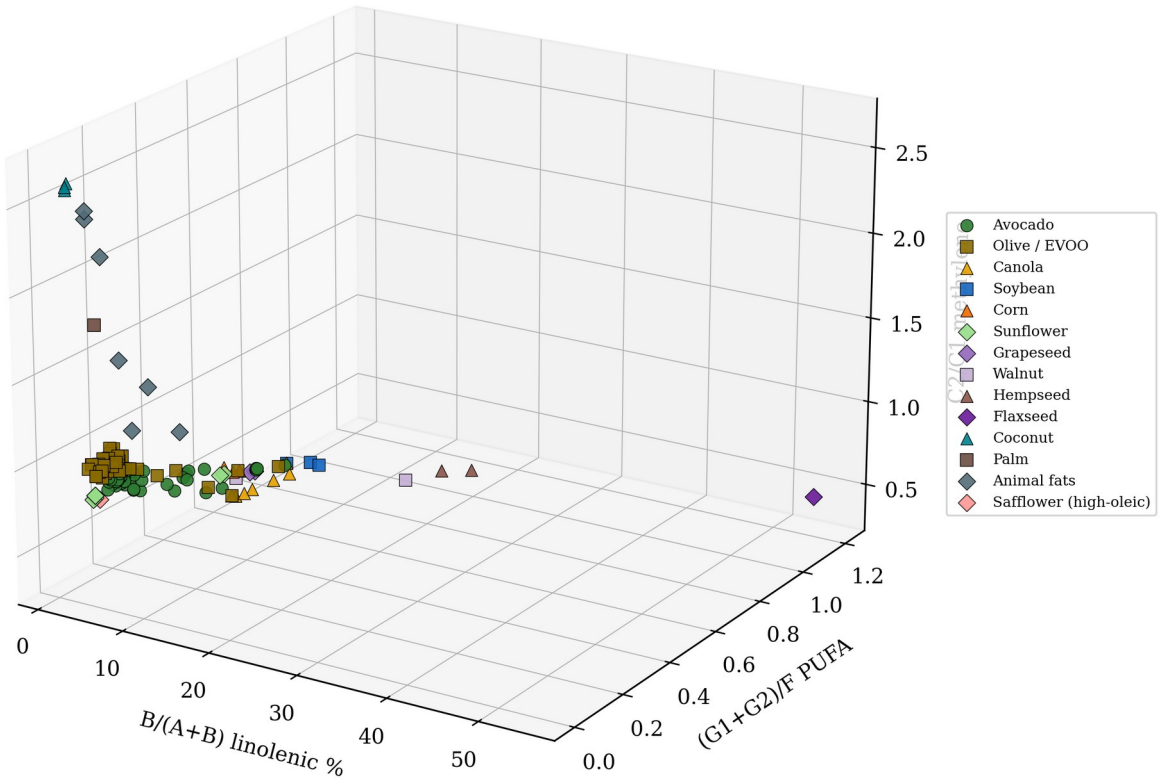

Figure 12. Three-dimensional identity map combining the linolenic marker B/(A+B), the polyunsaturation load (G1+G2)/F, and the bulk-methylene ratio C2/C1. The methylene axis separates the saturated fats from the unsaturated oils, while the linolenic and polyunsaturation axes resolve flaxseed, the linoleic oils, and the oleic oils.

5. Critical Assessment and Limitations

The candor that authentication work demands requires that the boundaries of the ten-region fingerprint be stated as plainly as its strengths. The most important limitation concerns the very discrimination that is analytically most valuable, the separation of avocado from olive oil and, more generally, of the several high-oleic oils from one another. The 93% cross-validated accuracy achieved for the avocado–olive pair is useful for screening but falls short of the certainty required for a forensic or regulatory conclusion, and it is achieved on subtle methylene-distribution and olefinic-fine-structure ratios whose reproducibility across instruments and operators has not been established in the present dataset. The decisive markers that distinguish these oils in definitive practice, chiefly squalene, the sterol profile, and the minor triterpene alcohols, resonate outside the integrated A-through-J window, in the aliphatic envelope below 2 ppm and

among weak resonances that are not resolved by routine integration [20, 28, 44]. A determination that an oleic oil is avocado rather than olive, or rather than high-oleic sunflower or safflower, should therefore be corroborated by a method sensitive to those minor components, whether by dedicated integration of the squalene resonances, by chromatography, or by both.

A second limitation attends the absolute quantification of linolenic acid at low levels. The ω-3 methyl region B does not fall to zero for oils that contain essentially no linolenic acid; a residual intensity on the order of a few units per triacylglycerol persists, arising from the tail of the main methyl envelope and from carbon-13 satellite intensity, and it imposes an apparent linolenic floor near three mole percent in oils such as avocado, olive, sunflower, and corn whose true linolenic content is below one percent. The consequence is that the derived linolenic percentages of Table 2 are accurate in their ordering and in their differences but carry a positive offset at the low end. The adulteration calibrations are unaffected by this offset, because they are constructed as displacements from the avocado base and the constant floor cancels, but any attempt to read absolute linolenic content for a low-linolenic oil from region B alone would overstate it, and this must be borne in mind when the parameter is used diagnostically.

Third, the composition of the reference set itself constrains the generality of the class centroids. Several classes are represented by only a small number of samples, soybean by three and a number of the specialty oils by one or two, so that their positions on the identity maps are indicative rather than definitive and should be reinforced with additional replicates before being used as fixed decision boundaries. The finding that the "sunflower" samples are of the high-oleic type is a reminder that a botanical label does not fix a fatty-acid profile, since modern cultivar development has produced high-oleic forms of sunflower, safflower, and other traditionally linoleic oils whose fingerprints overlap the oleic domain. The reference library should accordingly be understood as a snapshot of a particular retail population rather than as a canonical set of botanical archetypes.

Fourth, the adulteration calibrations rest on a single avocado base and on volumetric spike definitions. Real adulteration is heterogeneous: the authentic matrix varies from lot to lot, the adulterant may itself be a blend, and commercial substitution frequently co-varies minor components in ways that a controlled binary spike does not reproduce. The detection limits reported here, between 1.6 and 2.3 volume percent, therefore describe the intrinsic sensitivity of the spectroscopic measurement under favorable, well-defined conditions and should be regarded as a best case; the practical limit against an unknown authentic background, whose natural variability broadens the zero point, will be somewhat higher. The close correspondence between volumetric and mass fractions for these oils, within one to two percent, is a minor consideration by comparison but is noted for completeness.

Finally, the analysis is deliberately confined to the ten integrated regions as routinely reported, and it does not exploit the full resolution of the spectrum. Peak-fitting of overlapping multiplets, the inclusion of the diacylglycerol and free-fatty-acid resonances that report on hydrolytic quality [9], the sterol and squalene resonances that report on authenticity [20], and the aldehydic and hydroperoxide resonances that report on oxidation would each add orthogonal information, and their integration into the present framework represents the natural direction of further work. The strength of the ten-region approach is its speed and robustness for high-throughput screening; its complement is the targeted, higher-resolution measurement reserved for the samples that screening flags.

6. Conclusions and Recommendations

The reduction of the edible-oil ^{1}H NMR spectrum to ten integrated regions, normalized to the glyceryl methylene signal so that every intensity is expressed per triacylglycerol, yields a fingerprint from which the molar fatty-acid composition, the mean unsaturation, and the iodine value can be recovered by exact proton counting and validated against the compositional literature across some thirty oil and fat classes. A systematic combinatorial screen of the integrals and their ratios shows that authentication information is concentrated in three interpretable families: the linolenic markers B and G1, which separate the linolenic-bearing oils; the polyunsaturation markers G2 and the total bis-allylic intensity, which separate the linoleic oils; and the chain-distribution and olefinic-fine-structure ratios C1/D, C2/C1, and I/J, which resolve the oleic oils that the unsaturation markers cannot. Principal-component analysis captures 84.9 percent of the variance in three components and reproduces the same structure without supervision, and a leave-one-out discriminant model classifies the reference classes at 83.8 percent, with the avocado–olive pair separated at 93 percent by a three-ratio combination.

For routine screening the following diagnostic scheme is recommended as a distillation of these findings. An unknown oil is first placed on the master identity map of B/(A+B) against (G1+G2)/F, which assigns it to the oleic, linoleic, linolenic, or saturated domain. Within the oleic domain the ratios C2/C1, D/C1, and I/J are applied to distinguish olive, avocado, and the high-oleic seed oils, with the explicit understanding that a definitive avocado-versus-olive assignment requires orthogonal confirmation by squalene or sterol analysis. Where adulteration of an oleic oil is suspected, the coordinates G1/G2 and (G1+G2)/F identify the adulterant class by the direction of displacement from the authentic base, canola to the right, soybean upward, and palm downward, and the corresponding calibrations quantify the level of substitution to a detection limit near two volume percent. Applied in this sequence, the ten-region fingerprint provides a rapid, non-destructive, and quantitatively defensible first tier of edible-oil authentication, whose flagged samples are then referred to the targeted higher-resolution and chromatographic methods that furnish confirmatory proof.

References

1. Miyake, Y.; Yokomizo, K.; Matsuzaki, N. Determination of Unsaturated Fatty Acid Composition by High-Resolution Nuclear Magnetic Resonance Spectroscopy. *J. Am. Oil Chem. Soc.* **1998**, *75*, 1091–1094. DOI: 10.1007/s11746-998-0118-4.

2. Knothe, G.; Kenar, J. A. Determination of the Fatty Acid Profile by ^{1}H-NMR Spectroscopy. *Eur. J. Lipid Sci. Technol.* **2004**, *106*, 88–96. DOI: 10.1002/ejlt.200300880.

3. Guillén, M. D.; Ruiz, A. High Resolution ^{1}H Nuclear Magnetic Resonance in the Study of Edible Oils and Fats. *Trends Food Sci. Technol.* **2001**, *12*, 328–338. DOI: 10.1016/S0924-2244(01)00101-7.

4. Guillén, M. D.; Ruiz, A. Edible Oils: Discrimination by ^{1}H Nuclear Magnetic Resonance. *J. Sci. Food Agric.* **2003**, *83*, 338–346. DOI: 10.1002/jsfa.1317.

5. Barison, A.; da Silva, C. W. P.; Campos, F. R.; Simonelli, F.; Lenz, C. A.; Ferreira, A. G. A Simple Methodology for the Determination of Fatty Acid Composition in Edible Oils through ^{1}H NMR Spectroscopy. *Magn. Reson. Chem.* **2010**, *48*, 642–650. DOI: 10.1002/mrc.2629.

6. Castejón, D.; Mateos-Aparicio, I.; Molero, M. D.; Cambero, M. I.; Herrera, A. Evaluation and Optimization of the Analysis of Fatty Acid Types in Edible Oils by ^{1}H-NMR. *Food Anal. Methods* **2014**, *7*, 1285–1297. DOI: 10.1007/s12161-013-9747-9.

7. Castejón, D.; Fricke, P.; Cambero, M. I.; Herrera, A. Automatic ^{1}H-NMR Screening of Fatty Acid Composition in Edible Oils. *Nutrients* **2016**, *8*, 93. DOI: 10.3390/nu8020093.

8. Rossetto, G.; Kiraly, P.; Castañar, L.; Morris, G. A.; Nilsson, M. Improved Quantification by Nuclear Magnetic Resonance Spectroscopy of the Fatty Acid Ester Composition of Extra Virgin Olive Oils. *ACS Food Sci. Technol.* **2022**, *2*, 1237–1242. DOI: 10.1021/acsfoodscitech.2c00057.

9. Di Pietro, M. E.; Mannu, A.; Mele, A. NMR Determination of Free Fatty Acids in Vegetable Oils. *Processes* **2020**, *8*, 410. DOI: 10.3390/pr8040410.

10. Kim, W. W.; Rho, H. S.; Hong, Y. D.; Yeom, M. H.; Shin, S. S.; Yi, J. G.; Lee, M.-S.; Park, H. Y.; Cho, D. H. Determination and Comparison of Seed Oil Triacylglycerol Composition of Various Soybeans (*Glycine max* (L.)) Using ^{1}H-NMR Spectroscopy. *Molecules* **2013**, *18*, 14448–14454. DOI: 10.3390/molecules181114448.

11. Li, Q.; Cai, S.; Xu, D.; Lin, J.; Shen, G.; Feng, J. Comparative Analysis of Nutritional Composition Between GM and Non-GM Soybeans and Soybean Oils by NMR and GC-FID Techniques. *Food Anal. Methods* **2023**, *16*, 478–490. DOI: 10.1007/s12161-022-02435-8.

12. Sacchi, R.; Addeo, F.; Paolillo, L. ^{1}H and ^{13}C NMR of Virgin Olive Oil. An Overview. *Magn. Reson. Chem.* **1997**, *35*, S133–S145. DOI: 10.1002/(SICI)1097-458X(199712)35:13<S133::AID-OMR213>3.0.CO;2-K.

13. Vlahov, G. Application of NMR to the Study of Olive Oils. *Prog. Nucl. Magn. Reson. Spectrosc.* **1999**, *35*, 341–357. DOI: 10.1016/S0079-6565(99)00015-1.

14. Mannina, L.; Sobolev, A. P. High Resolution NMR Characterization of Olive Oils in Terms of Quality, Authenticity and Geographical Origin. *Magn. Reson. Chem.* **2011**, *49*, S3–S11. DOI: 10.1002/mrc.2856.

15. Fauhl, C.; Reniero, F.; Guillou, C. ^{1}H NMR as a Tool for the Analysis of Mixtures of Virgin Olive Oil with Oils of Different Botanical Origin. *Magn. Reson. Chem.* **2000**, *38*, 436–443. DOI: 10.1002/1097-458X(200006)38:6<436::AID-MRC672>3.0.CO;2-X.

16. García-González, D. L.; Mannina, L.; D'Imperio, M.; Segre, A. L.; Aparicio, R. Using ^{1}H and ^{13}C NMR Techniques and Artificial Neural Networks to Detect the Adulteration of Olive Oil with Hazelnut Oil. *Eur. Food Res. Technol.* **2004**, *219*, 545–548. DOI: 10.1007/s00217-004-0996-0.

17. Vigli, G.; Philippidis, A.; Spyros, A.; Dais, P. Classification of Edible Oils by Employing ^{31}P and ^{1}H NMR Spectroscopy in Combination with Multivariate Statistical Analysis. A Proposal for the Detection of Seed Oil Adulteration in Virgin Olive Oils. *J. Agric. Food Chem.* **2003**, *51*, 5715–5722. DOI: 10.1021/jf030100z.

18. Agiomyrgianaki, A.; Petrakis, P. V.; Dais, P. Detection of Refined Olive Oil Adulteration with Refined Hazelnut Oil by Employing NMR Spectroscopy and Multivariate Statistical Analysis. *Talanta* **2010**, *80*, 2165–2171. DOI: 10.1016/j.talanta.2009.11.024.

19. Šmejkalová, D.; Piccolo, A. High-Power Gradient Diffusion NMR Spectroscopy for the Rapid Assessment of Extra-Virgin Olive Oil Adulteration. *Food Chem.* **2010**, *118*, 153–158. DOI: 10.1016/j.foodchem.2009.04.088.

20. Hatzakis, E.; Dagounakis, G.; Agiomyrgianaki, A.; Dais, P. A Facile NMR Method for the Quantification of Total, Free and Esterified Sterols in Virgin Olive Oil. *Food Chem.* **2010**, *122*, 346–352. DOI: 10.1016/j.foodchem.2010.02.043.

21. Zamora, R.; Alba, V.; Hidalgo, F. J. Use of High-Resolution ^{13}C Nuclear Magnetic Resonance Spectroscopy for the Screening of Virgin Olive Oils. *J. Am. Oil Chem. Soc.* **2001**, *78*, 89–94. DOI: 10.1007/s11746-001-0225-z.

22. Zamora, R.; Gómez, G.; Hidalgo, F. J. Classification of Vegetable Oils by High-Resolution ^{13}C NMR Spectroscopy Using Chromatographically Obtained Oil Fractions. *J. Am. Oil Chem. Soc.* **2002**, *79*, 267–272. DOI: 10.1007/s11746-002-0472-z.

23. Garcia, R.; Pires, A.; Martins, N.; Carvalho, T.; Burke, A. J.; Cabrita, M. J. Assessment of the Triacylglycerol Fraction of Olive Oil by 1D-NMR Spectroscopy: Exploring the Usefulness of DEPT Tool on the Peak Assignments of ^{13}C NMR Spectra. *Eur. Food Res. Technol.* **2019**, *245*, 2479–2488. DOI: 10.1007/s00217-019-03359-0.

24. Lia, F.; Vella, B.; Zammit Mangion, M.; Farrugia, C. Application of ^{1}H and ^{13}C NMR Fingerprinting as a Tool for the Authentication of Maltese Extra Virgin Olive Oil. *Foods* **2020**, *9*, 689. DOI: 10.3390/foods9060689.

25. Cabrita, M. J.; Pires, A.; Burke, A. J.; Garcia, R. Seeking a Fast Screening Method of the Varietal Origin of Olive Oil: The Usefulness of an NMR-Based Approach. *Foods* **2021**, *10*, 399. DOI: 10.3390/foods10020399.

26. Ray, C. L.; Gawenis, J. A.; Greenlief, C. M. A New Method for Olive Oil Screening Using Multivariate Analysis of Proton NMR Spectra. *Molecules* **2022**, *27*, 213. DOI: 10.3390/molecules27010213.

27. Ok, S. Fast Screening of Turkish Olive Oil by NMR Spectroscopy for Geographical Determination and Discrimination Purposes. *Grasas Aceites* **2014**, *65*, e024. DOI: 10.3989/gya.122413.

28. Tang, F.; Green, H. S.; Wang, S. C.; Hatzakis, E. Analysis and Authentication of Avocado Oil Using High Resolution NMR Spectroscopy. *Molecules* **2021**, *26*, 310. DOI: 10.3390/molecules26020310.

29. Jin, H.; Wang, Y.; Lv, B.; Zhang, K.; Zhu, Z.; Zhao, D.; Li, C. Rapid Detection of Avocado Oil Adulteration Using Low-Field Nuclear Magnetic Resonance. *Foods* **2022**, *11*, 1134. DOI: 10.3390/foods11081134.

30. Tang, F.; Banker, T.; Green, H. S.; Wang, S. C.; Hatzakis, E. Analysis and Authentication of Avocado Oil by Low-Field Benchtop NMR Spectroscopy and Chemometrics. *J. Food Sci.* **2024**, *89*, 4276–4285. DOI: 10.1111/1750-3841.17142.

31. Hama, J. R.; Fitzsimmons-Thoss, V. Determination of Unsaturated Fatty Acids Composition in Walnut (*Juglans regia* L.) Oil Using NMR Spectroscopy. *Food Anal. Methods* **2022**, *15*, 1226–1236. DOI: 10.1007/s12161-021-02203-0.

32. Qian, J.; Zhao, C.; Zhu, H.; Tong, J.; Zhao, X.; Yang, H.; Guo, H. NMR Detection of Fatty Acids Content in Walnut Oil and Compared with Liquid Chromatography. *J. Food Meas. Charact.* **2021**, *15*, 2716–2726. DOI: 10.1007/s11694-021-00813-0.

33. Ramsay, A.; Fliniaux, O.; Fang, J.; Molinié, R.; Roscher, A.; Grand, E.; Guillot, X.; Kovensky, J.; Fliniaux, M.-A.; Schneider, B.; Mesnard, F. Development of an NMR Metabolomics-Based Tool for Selection of Flaxseed Varieties. *Metabolomics* **2014**, *10*, 1258–1267. DOI: 10.1007/s11306-014-0664-8.

34. Figueiredo, P. S.; Martins, T. N.; Ravaglia, L. M.; Alcantara, G. B.; Guimarães, R. C. A.; Freitas, K. C.; Nunes, Â. A.; de Oliveira, L. C. S.; Cortês, M. R.; Michels, F. S.; Toffoli-Kadri, M. C.; Bonfá, I. S.; Filiú, W. F. O.; Asato, M. A.; de Faria, B. B.; do Nascimento, V. A.; Hiane, P. A. Linseed, Baru, and Coconut Oils: NMR-Based Metabolomics, Leukocyte Infiltration Potential In Vivo, and Their Oil Characterization. Are There Still Controversies? *Nutrients* **2022**, *14*, 1161. DOI: 10.3390/nu14061161.

35. Parker, T.; Limer, E.; Watson, A. D.; Defernez, M.; Williamson, D.; Kemsley, E. K. 60 MHz ^{1}H NMR Spectroscopy for the Analysis of Edible Oils. *TrAC, Trends Anal. Chem.* **2014**, *57*, 147–158. DOI: 10.1016/j.trac.2014.02.006.

36. Ok, S. Detection of Olive Oil Adulteration by Low-Field NMR Relaxometry and UV–Vis Spectroscopy upon Mixing Olive Oil with Various Edible Oils. *Grasas Aceites* **2017**, *68*, e173. DOI: 10.3989/gya.0678161.

37. Wang, X.; Wang, G.; Hou, X.; Nie, S. A Rapid Screening Approach for Authentication of Olive Oil and Classification of Binary Blends of Olive Oils Using Low-Field Nuclear Magnetic Resonance Spectra and Support Vector Machine. *Food Anal. Methods* **2020**, *13*, 1894–1905. DOI: 10.1007/s12161-020-01799-z.

38. Huang, Z.-M.; Xin, J.-X.; Sun, S.-S.; Li, Y.; Wei, D.-X.; Zhu, J.; Wang, X.-L.; Wang, J.; Yao, Y.-F. Rapid Identification of Adulteration in Edible Vegetable Oils Based on Low-Field Nuclear Magnetic Resonance Relaxation Fingerprints. *Foods* **2021**, *10*, 3068. DOI: 10.3390/foods10123068.

39. Zhang, Q.; Saleh, A. S. M.; Shen, Q. Discrimination of Edible Vegetable Oil Adulteration with Used Frying Oil by Low Field Nuclear Magnetic Resonance. *Food Bioprocess Technol.* **2013**, *6*, 2562–2570. DOI: 10.1007/s11947-012-0826-5.

40. Ravaglia, L. M.; Pizzotti, A. B. C.; Alcantara, G. B. NMR-Based and Chemometric Approaches Applicable to Adulteration Studies for Assessment of the Botanical Origin of Edible Oils. *J. Food Sci. Technol.* **2019**, *56*, 507–511. DOI: 10.1007/s13197-018-3485-3.

41. Cai, S.; Zhang, Y.; Xia, F.; Shen, G.; Feng, J. An Expert System Based on ^{1}H NMR Spectroscopy for Quality Evaluation and Adulteration Identification of Edible Oils. *J. Food Compos. Anal.* **2019**, *84*, 103316. DOI: 10.1016/j.jfca.2019.103316.

42. Alexandri, E.; Ahmed, R.; Siddiqui, H.; Choudhary, M. I.; Tsiafoulis, C. G.; Gerothanassis, I. P. High Resolution NMR Spectroscopy as a Structural and Analytical Tool for Unsaturated Lipids in Solution. *Molecules* **2017**, *22*, 1663. DOI: 10.3390/molecules22101663.

43. Dais, P.; Hatzakis, E. Quality Assessment and Authentication of Virgin Olive Oil by NMR Spectroscopy: A Critical Review. *Anal. Chim. Acta* **2013**, *765*, 1–27. DOI: 10.1016/j.aca.2012.12.003.

44. Maestrello, V.; Solovyev, P.; Bontempo, L.; Mannina, L.; Camin, F. Nuclear Magnetic Resonance Spectroscopy in Extra Virgin Olive Oil Authentication. *Compr. Rev. Food Sci. Food Saf.* **2022**, *21*, 4056–4075. DOI: 10.1111/1541-4337.13005.

45. Hatzakis, E. Nuclear Magnetic Resonance (NMR) Spectroscopy in Food Science: A Comprehensive Review. *Compr. Rev. Food Sci. Food Saf.* **2019**, *18*, 189–220. DOI: 10.1111/1541-4337.12408.

46. Mannina, L.; Sobolev, A. P.; Viel, S. Liquid State ^{1}H High Field NMR in Food Analysis. *Prog. Nucl. Magn. Reson. Spectrosc.* **2012**, *66*, 1–39. DOI: 10.1016/j.pnmrs.2012.02.001.

47. Sobolev, A. P.; Ingallina, C.; Spano, M.; Di Matteo, G.; Mannina, L. NMR-Based Approaches in the Study of Foods. *Molecules* **2022**, *27*, 7906. DOI: 10.3390/molecules27227906.

Summary

This white paper has demonstrated that the routine ten-region integration of the ¹H NMR spectrum of an edible oil, when normalized to the glyceryl methylene signal so as to place every integral on a per-triacylglycerol basis, constitutes a quantitatively rigorous and combinatorially rich fingerprint of acyl-chain composition. Exact proton counting converts the integrals into molar fatty-acid fractions and an iodine value that reproduce accepted compositional ranges across approximately thirty oil and fat classes, from coconut at an iodine value near 5 to flaxseed near 182. A systematic screen of one hundred fifty-seven integral combinations localizes the authentication information within three chemically interpretable families of markers, and principal-component and discriminant analyses confirm that the resulting structure classifies the reference oils with an accuracy of 84 percent overall and separates the demanding avocado–olive pair at 93 percent by a compact three-ratio model. Gravimetric spiking of avocado oil with canola, soybean, and palm oils shows that each adulterant displaces the fingerprint along a distinct and identifiable vector, that the displacement is linear with detection limits between 1.6 and 2.3 volume percent, and that the same coordinates expose undisclosed base-oil substitution in commercial blends. The limitations of the approach have been stated without embellishment, chief among them the residual overlap of the high-oleic oils, the additive baseline that constrains absolute linolenic quantification, and the location of the decisive squalene and sterol markers outside the integrated window, and orthogonal confirmation has been recommended for any determination that must carry evidentiary weight. Within those boundaries, the ten-region ¹H NMR fingerprint offers a fast, non-destructive, and defensible foundation for the quality assessment and authentication of edible oils.

Prepared by Process NMR Associates, LLC — 84 Patrick Lane, Suite 115, Poughkeepsie, NY 12603 — www.process-nmr.com